

Electrochemical Corrosion Investigations on Binary and Ternary Zinc Alloy Coatings using Gel Electrolytes

Martin Babutzka,* Sven Grabowski, Holger Sahrhage, and Thomas Lampke

Novel agar-based test electrolytes are used to perform electrochemical corrosion investigations on ZnFe and ZnNi binary as well as ZnFeMo ternary zinc coatings. The objectives of the electrochemical investigations include the characterization of the corrosion behavior, the description of the protective effect of the coatings as well as the investigation of the layer formation and degradation under artificial aging. ZnFe and ZnFeMo coatings are applied with varying iron content as well as an additional passivation layer, respectively, to study the effect on corrosion resistance. The results show that the protective effect of the coatings is not negatively influenced by different iron contents or the addition of molybdenum. Additional passivation of the ZnFe-containing coatings by means of a passivating agent leads to a significant improvement in the protective effect. Artificial aging leads to a slight degradation of the additional passivation layer whereas coatings without post-treatment enhance their protective effect by the formation of corrosion product layers.

atmosphere are directly linked to the formation and dissolution kinetics of protective layers of adherent corrosion products. With an optimal interaction and a favorable sequence of atmospheric influencing factors, protective layers form over a long time period. These layers can be almost insoluble when exposed to moisture. They strongly inhibit the further dissolution of a zinc coating. Therefore, they are of decisive importance for the durability of corrosion protection. Kinetics of the formation and degradation of the corrosion product layers under service conditions lay the foundations for a long life cycle of zinc. To fully describe the temporal change of these processes, special attention is paid to the initial stage of corrosion product formation.^[1,2] The formed corrosion products

still show high reaction kinetics in this time period and can quickly transform or dissolve under changed corrosion conditions.

For years, a significantly accelerated development of new zinc coatings and alloys for ensuring corrosion protection under service conditions has been observed. In particular, ZnAl, ZnMg, and ZnAlMg coatings are being extensively researched and their corrosion behavior is described.^[3–7] Research is also driven by new REACH standards, as a result of which new variants such as ZnW and ZnWCu coatings are being developed.^[8] Research is also focusing on other variants such as ZnNi, ZnCo and ZnFe coatings,^[9,10] ZnMo coatings,^[11] and ZnFeMo coatings.^[12] In automotive engineering, ZnNi coatings are a standard, but are viewed critically due to REACH regulations and attempts are being made to substitute them.^[13]

With the help of corrosion tests in artificial climates, attempts are made to simulate the atmospheric corrosion of zinc and zinc coatings in an accelerated manner in the laboratory by using more corrosive parameters. This approach is intended to provide information on the corrosion protection and durability of zinc coatings with different alloy contents within short periods of time. ISO 14713-1^[14] restricts that no realistic result can be achieved with galvanized steel by means of salt spray tests according to ISO 9227.^[15] This is attributed to the lack of wet/dry cycles, without which no protective layer of corrosion products can be formed, resulting in continuous dissolution of the zinc layer. In 1964, Bartoň and Čermáková described in an article about the influence of corrosion products on atmospheric corrosion behavior that results of accelerated corrosion tests show no correlation with the corrosion behavior in natural atmospheres. They describe that without justification by kinetic principles and by the formation mechanism of corrosion products, the evaluability

1. Introduction


Zinc materials and zinc coatings are of outstanding importance for corrosion protection applications under atmospheric conditions, especially in civil engineering and the automotive industry. The corrosion resistance and thus the durability in the

M. Babutzka
Bundesanstalt für Materialforschung und -prüfung (BAM)
Division 7.6 Corrosion and Corrosion Protection
Unter den Eichen 87, 12205 Berlin, Germany
E-mail: martin.babutzka@bam.de

S. Grabowski
Bundesanstalt für Materialforschung und -prüfung (BAM)
Division 6.1 Surface Analysis and Interfacial Chemistry
Unter den Eichen 44-46, 12203 Berlin, Germany

H. Sahrhage
MacDermid Enthone Industrial Solutions
COVENTYA GmbH
Stadtring Nordhorn 116, 33334 Gütersloh, Germany

T. Lampke
Institute of Materials Science and Engineering
Materials and Surface Engineering Group
Chemnitz University of Technology
09107 Chemnitz, Germany

 The ORCID identification number(s) for the author(s) of this article can be found under <https://doi.org/10.1002/adem.202101336>.

© 2022 The Authors. Advanced Engineering Materials published by Wiley-VCH GmbH. This is an open access article under the terms of the Creative Commons Attribution License, which permits use, distribution and reproduction in any medium, provided the original work is properly cited.

DOI: 10.1002/adem.202101336

of the results from accelerated tests is limited. The exaggerated impact intensity of individual test parameters as well as their incorrect combination distort reaction mechanisms.^[16]

To encounter the problem of the low informative value of salt spray tests and accelerated corrosion tests, new, adapted tests are being developed, especially in the automotive industry and quality assurance. These are intended to simulate specific corrosion scenarios and site conditions, such as maritime areas, to be able to assess new types of zinc coatings with regard to their protective effect. A broad overview of different accelerated tests is given by LeBozec et al.^[17] However, the experience of recent years shows that even the continuous variation and adaptation of the test conditions does not offer a fundamentally new approach for corrosion testing and for the evaluation of the protective effect of a coating.

For several years, the use of gel electrolytes for electrochemical corrosion investigations was established as a new approach to describe zinc and zinc coatings with regard to their corrosion protection. An electrochemical instrumentation of gel electrolytes enables deeper insights into electrochemical reactions and allows the determination of corrosion-relevant parameters as well as a comparison with typical bulk electrolytes.^[18,19] For example, Monrrabal et al. were able to demonstrate that gel electrolytes enable rapid stabilization of the corrosion potential on stainless steel.^[20,21] Especially in the case of atmospheric corrosion processes in the presence of a thin film of moisture on the surface of the metal, it is to be expected that gel electrolytes can provide more in-depth information compared to bulk electrolytes. Gel electrolytes have already been successfully used for zinc in preliminary work. By using gel electrolytes on atmospherically formed corrosion product layers on pure zinc, a new approach for the determination of the Stearn–Geary constant based on polarization resistances was developed.^[22] Langklotz et al. were able to show the basic mechanisms and the additional benefit of gel electrolytes in combination with spectroscopic methods for investigations on zinc corrosion products. Using minimally invasive linear polarization resistance measurements (LPR), thin and unstable natural corrosion products on zinc were detected in the initial stage. The corrosion product formation was traced after very short weathering periods of only a few hours.^[2] Valet et al. verified a methodology based on LPR measurements and defined Corrosion product layer resistances R_L . In combination with the gel electrolyte, this methodology enabled minimally invasive measurements on zinc surfaces. Electrochemical impedance spectroscopy (EIS) and analytical methods validated the results.^[23] A comprehensive introduction to advantages and drawbacks of gel electrolytes for utilization on zinc and zinc coatings was carried out in previous work.^[2,23] Monrrabal et al. also have also successfully used gel electrolytes for galvanized zinc and have been able to highlight the differences compared to a liquid electrolyte. It was shown that gel electrolytes inherit a lower aggressiveness than a liquid electrolyte with the same saline composition.^[24]

In this article, gel electrolytes are used to investigate the corrosion protection, protective effect, and electrochemical stability of nickel-free binary and ternary zinc coatings. For this purpose, ZnFe coatings with different iron and molybdenum content as well as different post-treatment are investigated and compared to a ZnNi coating. Kazimierczak et al. have shown that the addition of low molybdenum contents (0.5 wt%) to zinc coatings can increase the corrosion resistance by an order of magnitude

compared to pure zinc. They attributed this to a different process of corrosion in the initial stage and a refinement of the microstructure of the initial coating.^[11] Using gel electrolytes, the present study describes the stability of the coatings in the as-received state (initial state). The effect of an additional passivation of the surface by a passivating agent is additionally discussed. Subsequently, artificial aging in a climatic chamber with an adapted wet/dry cycle is carried out for selected coatings without intensification of the test parameters in order to evaluate corrosion product formation or degradation of the passivation.

2. Experimental Section

2.1. Test Specimen Preparation

The test specimens were standardized Q-panel test sheets made of low-alloyed steel with various zinc-containing coatings, which were provided by Coventya (COVENTYA GmbH, Germany). The coatings were electrodeposited at 22 °C for 45 min at 1 A dm⁻² cathodic current density from the following alkaline electrolytes:

ZnFe (0.6%Fe):	Sodium hydroxide, 120 g l ⁻¹ (3 mol l ⁻¹) Zinc, 16 g l ⁻¹ (0.24 mol l ⁻¹) Iron [*] , 0.4 g l ⁻¹ (7.2 mmol l ⁻¹) PERFORMA 269 Base ^{**} , 89 ml l ⁻¹ PERFORMA 269 Brightener RAC ^{***} , 8 ml l ⁻¹ PERFORMA 269 Additive 10 ^{**} , 1 ml l ⁻¹ PERFORMA 269 Additive RP ^{**} , 11 ml l ⁻¹ [*] added as Fe(III) sulfate ^{**}) proprietary mixture of organic additives to improve deposition properties ^{***}) contains the Fe complexing agent (triethanolamine)
ZnFe (1.5%Fe):	Sodium hydroxide, 120 g l ⁻¹ (3 mol l ⁻¹) Zinc, 16 g l ⁻¹ (0.24 mol l ⁻¹) Iron [*] , 0.8 g l ⁻¹ (14.4 mmol l ⁻¹) PERFORMA 269 Base ^{**} , 89 ml l ⁻¹ PERFORMA 269 Brightener RAC ^{**} , 8 ml l ⁻¹ PERFORMA 269 Additive 10 ^{**} , 1 ml l ⁻¹ PERFORMA 269 Additive RP ^{***} , 11 ml l ⁻¹ [*] added as Fe(III) sulfate. ^{**}) proprietary mixture of organic additives to improve deposition properties. ^{***}) contains the Fe-complexing agent (triethanolamine).
ZnFeMo (0.6% Fe):	Sodium hydroxide, 120 g l ⁻¹ (3 mol l ⁻¹) Zinc, 16 g l ⁻¹ (0.24 mol l ⁻¹) Iron [*] , 0.4 g l ⁻¹ (7.2 mmol l ⁻¹) Molybdenum [*] , 12 g l ⁻¹ (0.13 mol l ⁻¹) PERFORMA 269 Brightener RAC ^{**} , 8 ml l ⁻¹ PERFORMA 269 Additive 10 ^{**} , 1 ml l ⁻¹ [*] added as Fe(III) sulfate and sodium molybdate pre-complexed with triethanolamine. ^{**}) proprietary mixture of organic additives to improve deposition properties.

ZnFeMo (1.5% Fe):	Sodium hydroxide, 120 g l ⁻¹ (3 mol l ⁻¹)
	Zinc, 16 g l ⁻¹ (0.24 mol l ⁻¹)
	Iron *), 0.8 g l ⁻¹ (14.4 mmol l ⁻¹)
	Molybdenum *), 12 g l ⁻¹ (0.13 mol l ⁻¹)
	PERFORMA 269 Brightener RAC **), 8 ml l ⁻¹
	PERFORMA 269 Additive 10 **), 1 ml l ⁻¹
	*) added as Fe(III) sulfate and sodium molybdate pre-complexed with triethanolamine.
	**) proprietary mixture of organic additives to improve deposition properties.
ZnNi 8%Ni):	Sodium hydroxide, 110 g l ⁻¹ (2.75 mol l ⁻¹)
	Zinc, 8 g l ⁻¹ (0.12 mol l ⁻¹)
	Nickel *), 1.8 g l ⁻¹ (30 mmol l ⁻¹)
	PERFORMA ZnNi 8% Additive **)
	*) added as Ni(II) sulfate.
	**) proprietary mixture of organic complexing agents and additives to improve deposition properties.

Table 1 gives an overview of the sample sheets and the different coatings with their respective alloy composition. The data provided for the iron, nickel, and molybdenum content refer to values determined by Coventya using inductively coupled plasma optical emission spectrometry (ICP-OES) and X-ray fluorescence. Coating thicknesses were measured by X-ray fluorescence with a FISCHERSCOPE X-ray XDV.

Two binary and two ternary ZnFe coatings were examined. The different coatings had an iron content of 0.6 or 1.5 wt% Fe, respectively. The ternary coatings were achieved by alloying of molybdenum. ICP-OES measurements revealed a content of 0.3–0.5 wt% Mo in the ternary coatings. In addition, a binary ZnNi coating with 8 wt% Ni was provided for comparative studies. All coatings were electrodeposited on the Q-panel test sheets by means of direct current (1 A dm⁻² for 45 min). Half of the test specimens were additionally passivated using the passivating agent FINDIP 145 CF (hereinafter referred to as: coating + passivation). FINDIP 145 CF is a cobalt-free passivate based on Cr(III) salts. The passivation was applied under the conditions such as concentration of 40 ml l⁻¹ FINDIP 145 CF, pH value of 2.0, temperature of 22 °C, and immersion time of 40 s.

Prior to electrochemical testing, specimens were cleaned, degreased, then rinsed with ethanol, and dried under a warm airflow.

In a first series of tests, the specimens were examined in the as-received state (initial state). To investigate the time-dependent aging behavior, test specimens of the coatings ZnFeMo(0.6%Fe) and ZnNi(8%Ni) were artificially weathered under the same conditions for 21 days in a climatic chamber of the type KB 300 from Liebisch Labortechnik. Each weathering cycle consisted of a humid phase (95% r. h. for 2 h, 28 °C) followed by a dry phase (60% r. h. for 4 h, 21 °C). Thus, 84 complete cycles were passed within 21 days, corresponding to 4 cycles per day. The cycles were chosen in such a way that there was no intensification of the test parameters. For the accompanying electrochemical

investigations, specimens were taken from the climatic chamber after the end of a drying phase.

2.2. Test Electrolyte for Electrochemical Corrosion Investigations

An agar-based gel electrolyte in the shape of circular gel pads was used as a test electrolyte for electrochemical investigations. To prepare the gel pads, 3 g of high-purity agar powder (agar with the designation “Ph Eur, BP” from Merck KGaA) was dissolved in 100 ml of deionized water, boiled to a temperature of ≈95–99 °C with constant stirring until complete clarification and cooled to ≈85 °C. The solution was then poured out onto a plastic plate for solidification. After solidification and formation of the gel network, the gel electrolyte had a gelatinous consistency and a dense surface without macroscopically detectable porosity. Afterward, it was cut to the desired dimensions for testing. Circular gel pads with a diameter of 19 mm—resulting in a measurement area of 2.84 cm²—and a pad thickness of about 3 mm were produced. Due to the raw agar material, the gel pads had a chloride content of 60 ppm (≈1.7 mM) and a pH value of 6–7 in the moisture film. A new gel pad was used for each measurement.

2.3. Measurement Setup

A three-electrode measurement setup according to Valet et al.^[23] was used for electrochemical corrosion investigations by means of gel electrolytes. An Ir/MMO anode was used as a counter electrode. A saturated silver/silver chloride reference electrode (+197 mV_{NHE}) was used as the reference electrode. The sample sheets were connected as the working electrode. The counter and working electrodes were arranged plane-parallel to each other with the gel electrolyte between them. The counter electrode is attached to the upper surface of the gel electrolyte with a constant pressure. A Gamry Instruments Interface 1000 potentiostat/galvanostat was used as the measuring system. The influence of the iR drop in the gel electrolyte can be neglected for the measurement setup, according to the results of Langklotz et al.^[2]

Table 1. Types of zinc coating, information on the type of post-treatment, and coating thickness.

Coating	Treatment	Coating thickness [μm]
ZnFe (0.6%Fe)	Coating without post-treatment	6.7 ± 0.7
	Coating + passivation	7.0 ± 0.7
ZnFe (1.5%Fe)	Coating without post-treatment	4.5 ± 0.2
	Coating + passivation	6.1 ± 0.1
ZnFeMo (0.6%Fe)	Coating without post-treatment	5.5 ± 0.4
	Coating + passivation	7.3 ± 0.2
ZnFeMo (1.5%Fe)	Coating without post-treatment	5.5 ± 0.2
	Coating + passivation	4.9 ± 0.5
ZnNi (8%Ni)	Coating without post-treatment	9.0 ± 0.0

2.4. Electrochemical Methods for the Determination of Corrosion-Relevant values

By using the described test setup, corrosion-relevant characteristic values were determined with various electrochemical methods. DC and AC polarization methods were used to describe the corrosion behavior and the structure of the coatings electrochemically.

Prior to polarization, the time-dependent course of the open-circuit potential E_{OCP} was recorded over a period of 300 s, beginning from the first electrolyte contact. E_{OCP} values given in the following diagrams were determined after 300 s of potential measurements and contact with the gel electrolyte. Potential measurements provide a first insight into the stability of the coatings in contact with the thin moisture film of the gel electrolytes.

After potential measurements, Corrosion product layer resistance R_L according to Valet et al. were determined by means of linear polarization. R_L values are characteristic values for the momentary protective effect of the coatings.^[23] For this purpose, starting from -5 mV versus E_{OCP} , polarization was carried out in the anodic direction up to a potential of +5 mV versus E_{OCP} with a sweep rate of 1 mV s^{-1} . In a potential range with a small deviation from the free corrosion potential ($\pm 3 \text{ mV vs } E_{\text{corr}}$), values were determined according to the following relationship (Equation (1)).

$$R_L = \frac{\Delta E}{\Delta i} \quad (1)$$

In addition, impedance spectra were recorded using EIS to electrochemically characterize the structure of the coatings.

A sinusoidal potential excitation with an amplitude of $\pm 7.75 \text{ mV}$ versus E_{OCP} was applied in a frequency range starting from 100 000 Hz down to 0.1 Hz. Ten measurement points per decade were recorded. The typical bode plots of the impedance curve and the phase angle are shown in the following diagrams. An EIS fit of the individual spectra was performed using Gamry Echem Analyst software. The spectra of the coatings were fitted with the equivalent circuit diagrams from **Figure 1** and assigned to the corresponding layer system.

R_{el} represents the electrolyte resistance, R_p the polarization resistance, $R_{\text{layer 1}}$ and $R_{\text{layer 2}}$ resistances of the different layers, W_d the Warburg impedance as diffusion component and CPE, $\text{CPE}_{\text{layer 1}}$ and $\text{CPE}_{\text{layer 2}}$ constant phase elements. A detailed extraction of all fit results and values was omitted, since the R_L values determined by means of dynamic polarization correlate well with the R_p values from EIS investigations.^[23]

All electrochemical measurements were carried out at room temperature. The experiments were repeated at least three times to ensure statistical relevance. Deviation ranges presented correspond to the minimum and maximum values measured.

2.5. Microscopic Investigations

Microscopic investigations were performed to display changes in the layer and surface morphology. Metallographic cross-sections were prepared, and SEM measurements were performed from the top view.

Metallographic cross-sections enabled characterization of the different coating layers and the corrosion product layers prior to and after aging. Representative samples were embedded,

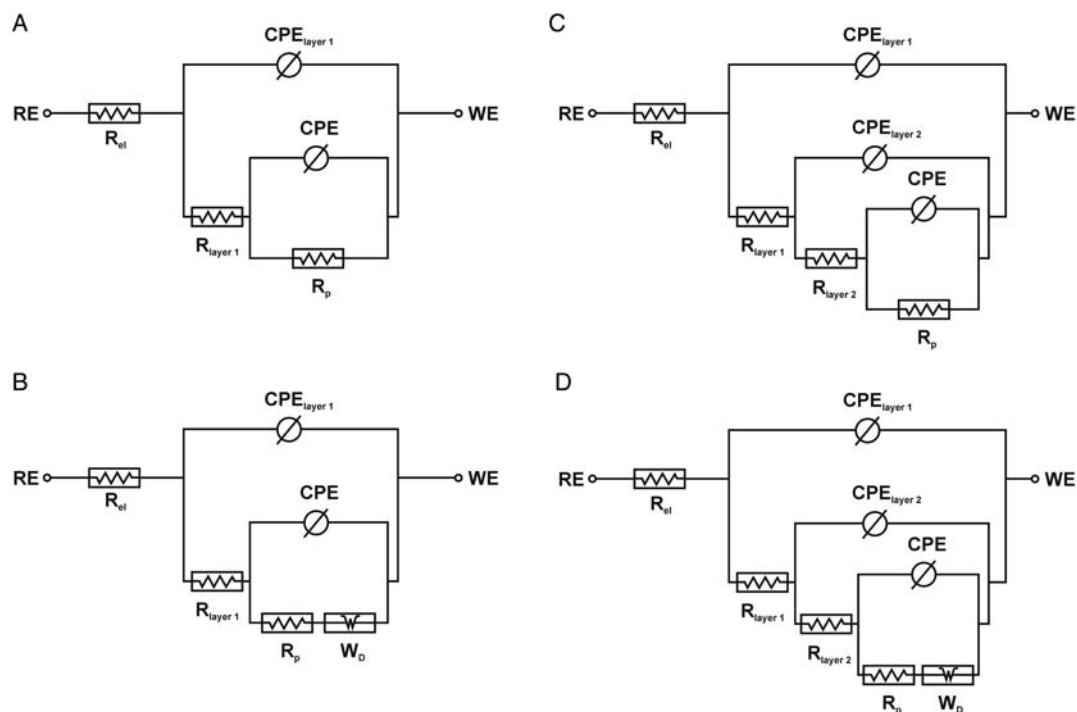


Figure 1. Equivalent circuit models used for EIS fitting of binary and ternary coatings. A) Equivalent circuit model including a coating layer. B) Equivalent circuit model including a coating layer and a diffusion component. C) Equivalent circuit model including several layers. D) Equivalent circuit model including several layers and a diffusion component.

mechanically ground, and polished with decreasing grit size. Subsequently, they were investigated by a light optical microscope Axioscope 7 from Carl Zeiss AG with $\times 1000$ magnification. Microscopic images of flat sections were prepared and assessed with respect to the aspect of aging and the morphology of corrosion phenomena.

For topographic analyses of the samples and the corrosion products, a Hitachi FLEX SEM 1000 compact scanning electron microscope (SEM) was used. The samples were investigated in the secondary electron detection mode to measure surface sensitivity. The acceleration voltage was set to 15 kV by a working distance of 10 mm for the best intensity yield. In addition, an ≈ 18 nm thin carbon layer was deposited with the Leica EM ACE600 high vacuum coating system to achieve better electrical conductivity.

3. Results

3.1. Coatings in Initial State

3.1.1. Layer and Surface Morphology

Metallographic cross-sections for coatings in the initial state are presented in **Figure 2**.

The bright layer represents the coating. The lower darker area is the steel substrate. The ZnFe-containing coatings in **Figure 2a, b** show no defects in the coating layer. The coatings have a homogeneous thickness. The passivation layer cannot be resolved by optical microscopy and is not visible in **Figure 2b**. **Figure 2c** shows the coating of ZnNi(8%Ni). The surface appears somewhat rougher. However, the coating is homogeneously deposited on the steel substrate and no defects are visible in the coating.

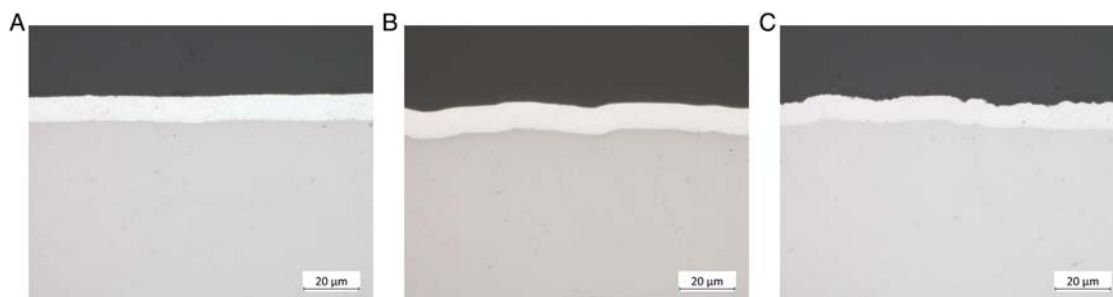


Figure 2. Metallographic crosssections of binary and ternary zinc coatings in the initial state, investigated by a light optical microscope, magnification $\times 1000$. A) ZnFe/ZnFeMo coating without post-treatment. B) ZnFe/ZnFeMo coating + passivation. C) ZnNi coating without post-treatment.

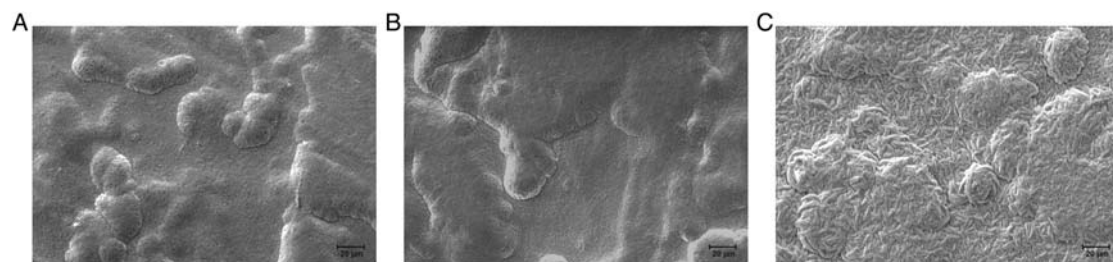


Figure 3. SEM images of binary and ternary zinc coatings in the initial state, top view. A) ZnFe/ZnFeMo coating without post-treatment. B) ZnFe/ZnFeMo coating + passivation. C) ZnNi coating without post-treatment.

SEM images from the top view of the coatings are shown in **Figure 3**.

It can be seen by image blurring during SEM measurements that, despite the carbon layer applied, no good conductivity was observed for the ZnFe/ZnFeMo-containing coatings (**Figure 3a, b**). The images show complete coverage of the substrates with the different coatings. No defects down to the substrate were observed. The passivation layer does not lead to a visible change in morphology (**Figure 3b**). The coating ZnNi(8%Ni) is built up with needle-shaped deposits (**Figure 3c**) and thus provides a different morphology than ZnFe/ZnFeMo-containing coatings.

3.1.2. Corrosion Potential Measurements

The course of the corrosion potential over a period of 300 s was measured and investigated on all coatings in the initial state. **Figure 4** shows potential versus time curves of the different binary and ternary coatings with and without additional passivation in contact to gel electrolytes. A representative potential curve per coating type is shown.

For all coatings, the corrosion potential lies in a potential range typical for zinc, independent of the post-treatment. For the coatings without post-treatment (**Figure 4a**), the potential shifts to more anodic values within the first 100 s and increases by ≈ 20 mV. Afterward, the potentials remain at a constant value. The different coatings do not show any differences with regard to the course of the potential curve, but the position of the potentials differs. The coatings ZnFe(0.6%Fe), ZnFe(1.5%Fe) and ZnFeMo(1.5%Fe) show a similar potential value. The coating ZnNi(8%Ni) is ≈ 50 mV more cathodic. The coating ZnFeMo(0.6%Fe) is ≈ 100 mV more anodic. For additionally passivated coatings (**Figure 4b**), the potential curve tends to start

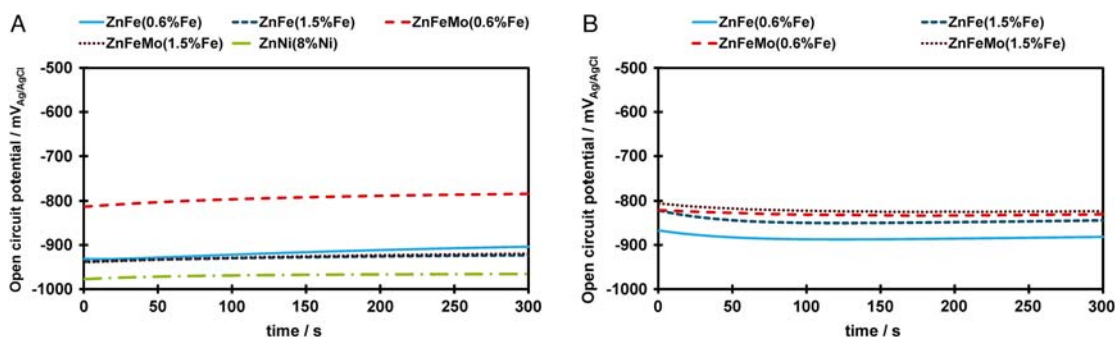


Figure 4. Open-circuit potential versus time curves of binary and ternary zinc coatings in the initial state over a period of 300 s, contact to a gel electrolyte. A) Coating without post-treatment. B) Coating + passivation.

more anodic and shifts to more cathodic values by ≈ 20 mV within the first 50 s. Afterward, the potential remains at a constant value. The passivated coatings do not show any significant differences with regard to the course of the potential curve and the position of the potentials. As one exception, the ZnFe(0.6%Fe) coating tends to be 50 mV more cathodic.

Figure 5 provides an overview of the E_{OCP} values of the different binary and ternary coatings with and without passivation after 300 s of contact to the gel electrolyte.

The E_{OCP} values of the passivated coatings are significantly more anodic than those of the coatings without additional passivation with the exception of ZnFeMo(0.6%Fe). For ZnFeMo(1.5%Fe), the E_{OCP} value of the passivated coating is ≈ 100 mV more anodic than the corresponding non-passivated coating. Of all the binary and ternary coatings examined, the E_{OCP} value of ZnNi(8%Ni) is the most cathodic. The E_{OCP} values of the coatings with 1.5 wt% Fe are more cathodic than those of the coatings with 0.6 wt% Fe. No coating lies in a potential range below -980 mV_{Ag/AgCl}, which would indicate an active zinc surface when in contact with a gel electrolyte.^[2,3]

3.1.3. Determination of Corrosion Product Layer Resistances R_L

Following the 300 s of potential measurement, R_L values of the coatings were determined according to Equation (1). After 300 s of potential measurement, there was no significant potential drift

influencing the R_L value. **Figure 6** summarizes the R_L values of the coatings in the initial state.

Coatings without post-treatment show R_L values between 12 and 15 k Ω cm². The deviation ranges of the individual measured values are extremely small. There are no significant differences between the different binary and ternary coatings. Furthermore, no influence of the iron content and from the addition of molybdenum is measurable. The passivated coatings show an R_L value that is tenfold higher than that of the respective untreated coatings. No influence of the iron content and from the addition of molybdenum can be detected.

3.1.4. EIS

EIS was carried out to characterize the layered structure of the coatings. **Figure 7** shows the impedance spectra and the corresponding phase shift for the different coatings at one representative example per coating.

The impedance spectra and frequency-dependent phase shifts show no significant differences between the different coatings without post-treatment (Figure 7a). In addition, the passivated coatings (Figure 7b) do not differ significantly from each other. Nevertheless, an influence of the passivation compared to the untreated coatings can be seen. The maximum of the phase shift changes to higher frequencies for the passivated surfaces compared to the untreated coatings. Higher impedances are

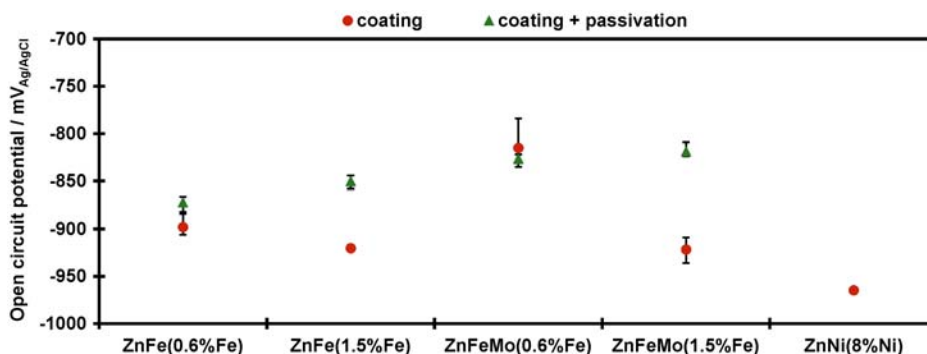


Figure 5. Open-circuit potential values E_{OCP} of binary and ternary zinc coatings in the initial state after 300 s of contact to a gel electrolyte, mean values, and deviation ranges.

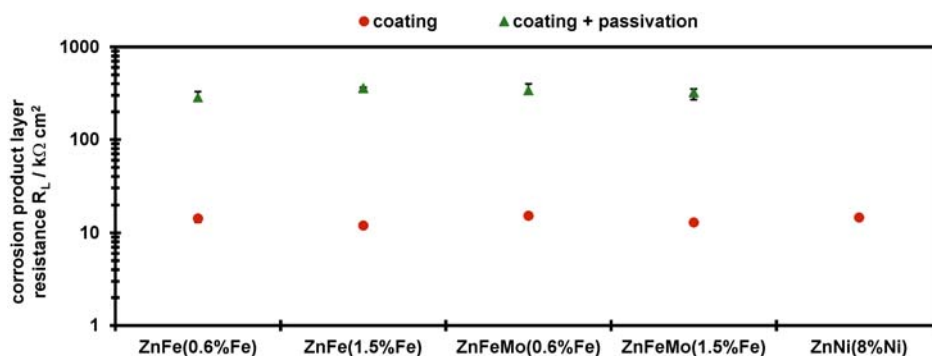


Figure 6. Corrosion product layer resistances R_L of binary and ternary zinc coatings in the initial state, determined after 300 s contact with a gel electrolyte, mean values, and deviation ranges.

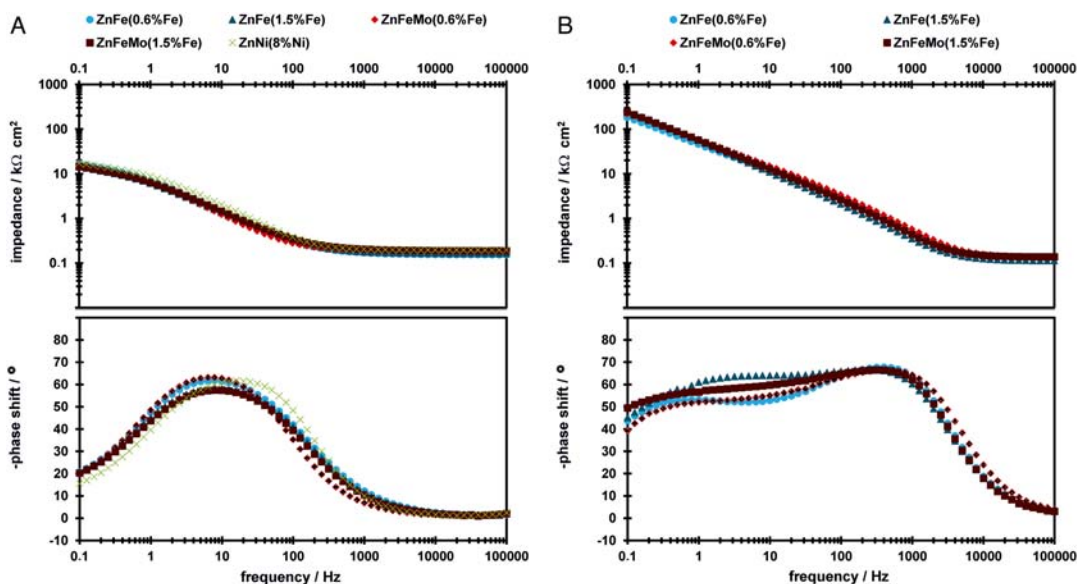


Figure 7. Impedance spectra and phase shift from EIS on binary and ternary zinc coatings in the initial state, contact with a gel electrolyte. A) Coating without post-treatment. B) Coating + passivation.

measured at lower excitation frequencies. In addition, the passivated coatings show 20° – 30° more positive phase shifts at lower excitation frequencies. **Table 2** gives an overview of the equivalent circuit models according to Figure 1, by which the coatings could be fitted and described most accurately. The fitting of the EIS data to equivalent circuit models and the extraction of kinetic parameters is performed in the Annex.

Binary and the ternary coatings without post-treatment can be assigned to the equivalent circuit model (A) “Equivalent circuit model including a coating layer” without exception. The passivated coatings have the most accurate fit by using equivalent circuit model (C) “Equivalent circuit model including several layers.” The additional second layer is the passivation layer. No layer system with an additional diffusion component (Warburg impedance) was determined in the initial state.

This article does not present the individual values and data of the EIS-fits in tabular form. It was shown by Valet et al. that the R_p values determined by means of equivalent circuit models

correlate well with the R_L values.^[23] Thus, no new findings would be provided regarding the protective effect of the coatings.

3.2. Artificial Aging in a Climatic Chamber

3.2.1. Layer and Surface Morphology

Metallographic cross-sections for coatings after 21 days of artificial aging are summarized in **Figure 8**.

The bright layer represents the coating. The lower darker area is the steel substrate. The ZnFe-containing coatings in Figure 8a, b show defects in the coating layer that reach down to the substrate. Coatings without post-treatment (Figure 8a) show corrosion phenomena after artificial aging. On top of the coating, a layer of corrosion products with a thickness of 5–10 μm can be seen in the cross-section. The passivation layer cannot be resolved by optical microscopy and is not visible in Figure 8b.

Table 2. Assignment of the EIS spectra of coatings from Figure 7 to the equivalent circuit models in Figure 1; Fitting results are provided in Table A1 and A3 in the Annex.

Coating	Treatment	Equivalent circuit model
ZnFe(0.6%Fe)	Coating without post-treatment	(A) Equivalent circuit model including a coating layer
	Coating + passivation	(C) Equivalent circuit model including several layers
ZnFe(1.5%Fe)	Coating without post-treatment	(A) Equivalent circuit model including a coating layer
	Coating + passivation	(C) Equivalent circuit model including several layers
ZnFeMo(0.6%Fe)	Coating without post-treatment	(A) Equivalent circuit model including a coating layer
	Coating + passivation	(C) Equivalent circuit model including several layers
ZnFeMo(1.5%Fe)	Coating without post-treatment	(A) Equivalent circuit model including a coating layer
	Coating + passivation	(C) Equivalent circuit model including several layers
ZnNi(8%Ni)	Coating without post-treatment	(A) Equivalent circuit model including a coating layer

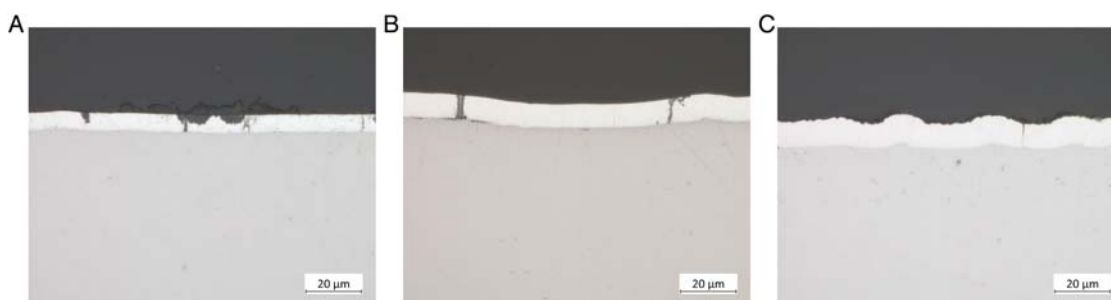


Figure 8. Metallographic cross-sections of binary and ternary zinc coatings after 21 days of artificial aging, investigated by a light optical microscope, magnification $\times 1000$. A) ZnFe/ZnFeMo coating without post-treatment. B) ZnFe/ZnFeMo coating + passivation. C) ZnNi coating without post-treatment.

Figure 8c shows the coating ZnNi(8%Ni). A small defect that reaches down to the substrate is visible. The coating shows no signs of extensive corrosion and is covered by a small layer of corrosion products with a thickness of $2 \mu\text{m}$.

SEM images from the top view of the coatings are presented in Figure 9.

It can be seen by image blurring while SEM measurements that, despite the carbon layer applied, no good conductivity was observed for the ZnFe/ZnFeMo-containing coatings with a passivation layer (Figure 9b) and the ZnNi(8%Ni) coating (Figure 9c). Figure 9a,c shows the coverage of the surface by corrosion products of coatings without post-treatment. The passivation layer does not lead to a visible change in morphology (Figure 9b).

3.2.2. Corrosion Potential Measurement

The ternary coating ZnFeMo(0.6%Fe) was selected for artificial aging in a climatic chamber in the variants without post-treatment and with passivation, as the various iron-containing binary and ternary coatings did not differ significantly in the electrochemical investigations in the initial state. This coating is, therefore, exemplary for the ZnFe-containing coatings. In addition, the binary coating ZnNi(8%Ni) was subjected to artificial aging for comparison. Figure 10 shows the potential versus time curves of the investigated coatings in contact with the gel electrolyte as a function of the artificial aging time in the climatic chamber.

In the case of the coating ZnFeMo(0.6%Fe) without post-treatment in Figure 10a, the corrosion potential lies in the initial



Figure 9. SEM images of binary and ternary zinc coatings after 21 days of artificial aging, top view. A) ZnFe/ZnFeMo coating without post-treatment. B) ZnFe/ZnFeMo coating + passivation. C) ZnNi coating without post-treatment.

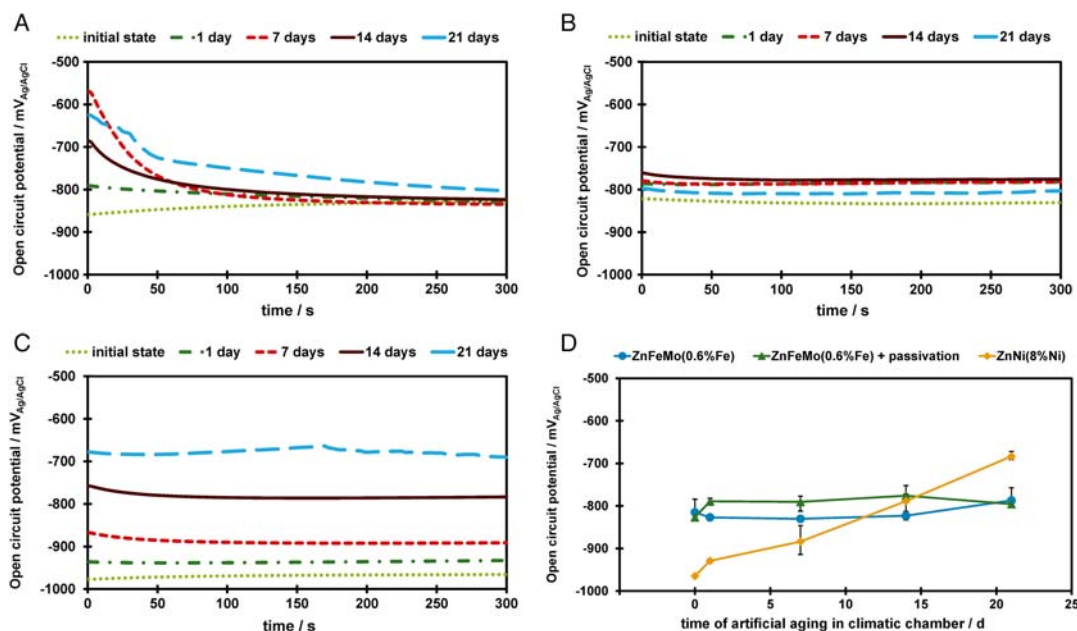


Figure 10. Open-circuit potential depending on artificial aging time, contact with a gel electrolyte. A) Potential versus time curves of ZnFeMo (0.6%Fe), coating without post-treatment. B) Potential versus time curves of ZnFeMo(0.6%Fe), coating + passivation. C) Potential versus time curves of ZnNi (8%Ni), coating without post-treatment. D) Open-circuit potential values E_{OCP} after 300 s, mean values, and deviation ranges.

state in a range typical for zinc. After 24 h of artificial aging in the climatic chamber, the potential shifts by ≈ 80 mV in anodic direction at the first electrolyte contact. With increasing weathering time, the corrosion potential shifts further in anodic direction at the first electrolyte contact. After 300 s of electrolyte contact, however, the corrosion potential is in a similar range for all weathering times. For the passivated variant of ZnFeMo(0.6% Fe) (Figure 10b), in contrast, the potential shifts slightly anodic after 24 h of artificial aging up to a value of -780 mV_{Ag/AgCl} and remains at this level. For the binary coating ZnNi(8%Ni) (Figure 10c), the corrosion potential shifts continuously in anodic direction with increasing artificial aging time. Values are reached that are far more anodic than -700 mV_{Ag/AgCl}. E_{OCP} values measured after 300 s (Figure 10d) confirm the described trends. The binary coating ZnNi(8%Ni) starts more cathodic than the two ZnFeMo coatings. With increasing artificial aging time, however, the potential values become more anodic than those of the ZnFeMo coatings. The ZnFeMo coatings show similar potential ranges, with the passivated variant showing slightly more anodic potentials. After 21 days of artificial aging, both variants inherit the same potential level of -800 mV_{Ag/AgCl}.

3.2.3. Determination of Corrosion Product-Layer Resistances R_L

Figure 11 shows the development of the determined R_L values depending on the artificial aging time in the climatic chamber after 300 s of potential measurement.

The R_L value of the coating ZnFeMo(0.6%Fe) without post-treatment initially drops slightly to values of 10 k Ω cm² within the first day of artificial aging. Subsequently, the R_L value

increases with increasing weathering duration up to 14 days to values above 100 k Ω cm². After 21 days, however, the R_L value drops again, but does not reach the low level of the initial state. Regarding the passivated coating ZnFeMo(0.6%Fe), the R_L value increases from 340 to 437 k Ω cm² within the first day. Afterward, it tends to decrease constantly. It is lower than in the initial state with values of 237 k Ω cm² after 21 days. Regarding the binary coating ZnNi(8%Ni), the R_L value constantly increases with increasing weathering duration up to 14 days to values of 174 k Ω cm². Subsequently, the R_L value decreases to values of 90 k Ω cm² after 21 days of artificial aging. The passivated coating has a higher R_L value than the other two variants within the entire weathering period of 21 days.

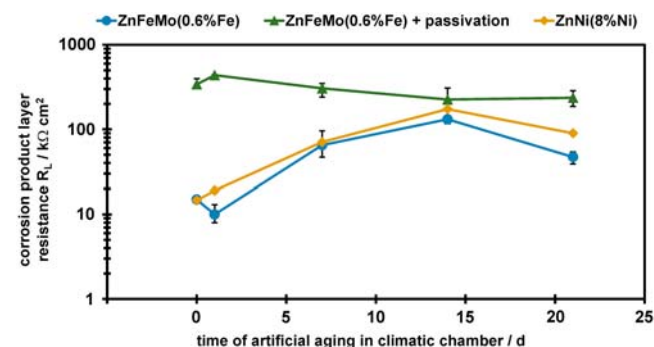


Figure 11. Corrosion product layer resistances R_L of ZnFeMo (0.6%Fe) with and without passivation and of ZnNi(8%Ni) as a function of the artificial aging time, determined after 300 s contact with a gel electrolyte, mean values, and deviation ranges.

3.2.4. EIS

The impedance spectra and the curves of the phase shifts from EIS are compared in **Figure 12** as a function of the weathering time in the climatic chamber.

Regarding the coating ZnFeMo(0.6%Fe) without post-treatment in Figure 12a, a strong dependence of impedance and phase shift on the weathering time is measurable. With increasing aging time in the climatic chamber, the impedance values tend to increase over the entire frequency range and there is a change of the maximum of the phase shift to higher excitation frequencies. An exception is the spectrum after one day of weathering. At this point, the impedance values are lower compared to the initial state. Regarding the passivated variant of ZnFeMo(0.6%Fe) in Figure 12b, the impedance spectra and phase shifts do not change significantly with increasing

weathering time in the climatic chamber. The impedance values tend to decrease slightly at low excitation frequencies and increasing weathering time compared to the initial state. Regarding the coating ZnNi(8%Ni) in Figure 12c, the impedance values tend to increase with increasing weathering time in the climatic chamber and there is a shift of the maximum of the phase angle to higher excitation frequencies. The course of the phase shift differs significantly in the range from 1 to 1000 Hz from the course of the coating ZnFeMo(0.6%Fe) without post-treatment. **Table 3** gives an overview of the equivalent circuit models according to Figure 1, by which the respective coatings could be fitted and described most accurately. The fitting of the EIS data to equivalent circuit models and the extraction of kinetic parameters is performed in the Annex.

There are differences in the time-dependent behavior of the three investigated coatings. For example, the coating

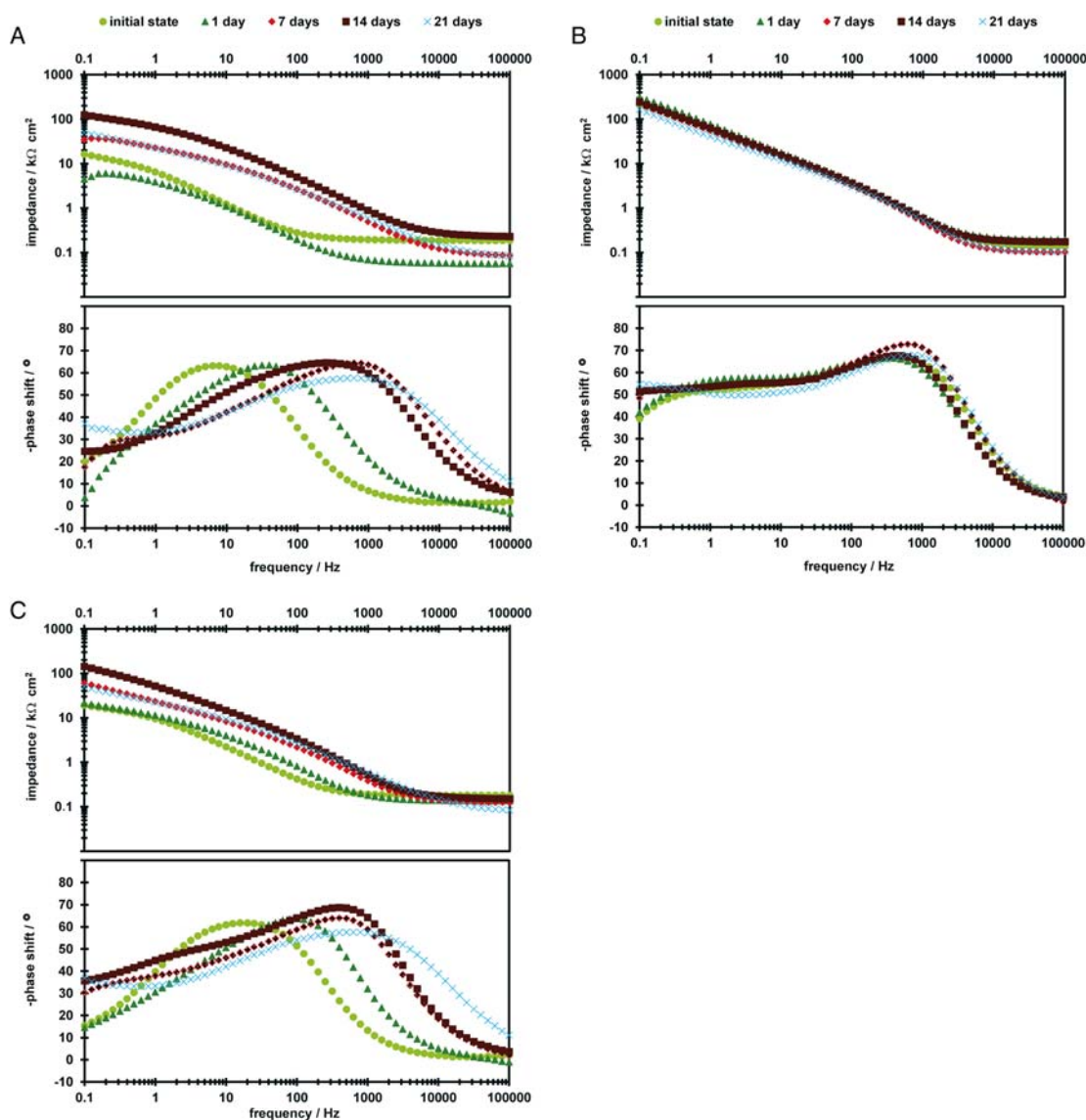


Figure 12. Impedance spectra and phase shift from EIS as a function of the artificial aging time, contact with a gel electrolyte. A) ZnFeMo (0.6%Fe), coating without post-treatment. B) ZnFeMo (0.6%Fe), coating + passivation. C) ZnNi (8%Ni), coating without post-treatment.

Table 3. Assignment of the EIS spectra of coatings from Figure 12 to the equivalent circuit models in Figure 1; Fitting results are provided in Table A1, A2, A3, and A4 in the annex.

Coating	Time of artificial aging	Equivalent circuit model
ZnFeMo(0.6%Fe) coating without post-treatment	Initial state	(A) Equivalent circuit model including a coating layer
	1 day	(B) Equivalent circuit model including a coating layer and a diffusion component
	7 days	(C) Equivalent circuit model including several layers
	14 days	(C) Equivalent circuit model including several layers
	21 days	(C) Equivalent circuit model including several layers
ZnFeMo(0.6%Fe) + passivation	Initial state	(C) Equivalent circuit model including several layers
	1 day	(C) Equivalent circuit model including several layers
	7 days	(C) Equivalent circuit model including several layers
	14 days	(C) Equivalent circuit model including several layers
	21 days	(C) Equivalent circuit model including several layers
ZnNi(8%Ni)	Initial state	(A) Equivalent circuit model including a coating layer
	1 day	(B) Equivalent circuit model including a coating layer and a diffusion component
	7 days	(B) Equivalent circuit model including a coating layer and a diffusion component
	14 days	(C) Equivalent circuit model including several layers
	21 days	(D) Equivalent circuit model including several layers and a diffusion component

ZnFeMo(0.6%Fe) without post-treatment changes from a coating layer (A) in the initial state to a coating layer with an additional diffusion component (B) after one day of artificial aging. With increasing aging time, an additional layer is measured (C). For the passivated variant, the equivalent circuit model does not change with increasing aging time. It remains a model with two layers (C), whereby one of the two layers is the passivation. The coating ZnNi(8%Ni) experiences the greatest changes in the layer structure with increasing aging time. Starting from the equivalent circuit diagram with a coating layer (A) in the initial state, an additional diffusion component (B) is added after one day of weathering. This layer structure is also measured after 7 days. After 14 days of weathering, a coating system with two layers (C) has formed, whereby the additional layer is formed by corrosion products. After 21 days of weathering, a diffusion component (D) is added to this layer structure.

4. Discussion

4.1. Influence of Varying Fe Content and Mo Addition on Corrosion Behavior

The results of the potential measurements in Figure 4a and 5 show that an increase in the iron content of the coatings from 0.6 to 1.5 wt% Fe leads to a shift of the open-circuit potential E_{OCP} in the cathodic direction for both the binary and the ternary coatings. However, an influence on the protective effect and the electrochemical stability of the coatings in the initial state cannot be detected, as the R_L values in Figure 6 prove. The values of all binary and ternary coatings lie in a range of 12–15 $\text{k}\Omega\text{cm}^2$ and thus do not differ significantly. The values are within a typical range for zinc surfaces that have not been exposed to natural or artificial weathering.^[2,23] The ZnNi coating used for comparison shows a significantly more cathodic potential than the binary

and ternary ZnFe-containing coatings, but the protective effect and stability corresponding to the R_L values are at the same level. Based on the EIS investigations, no influence of the different iron contents of the binary and ternary coatings can be determined. The impedance spectra and phase shifts (Figure 7) are similar, and the coatings can be modeled with the same equivalent circuit model. All coatings show a typical system with a coating layer independent of the iron content of the alloy, which furthermore does not differ from the investigated ZnNi coating. The difference in surface morphology between ZnFe-containing coatings and ZnNi coating detected by SEM images (Figure 3a,c) does not influence EIS results and fitting significantly. Overall, the results show that an increasing iron content initially only affects the E_{OCP} values. In contrast, the protective effect, electrochemical stability, and structure of the coating system are not influenced by different iron contents.

The ternary coatings were produced by adding molybdenum. This results in a molybdenum content of 0.3–0.5 wt% Mo in the coatings. At a low iron content of 0.6 wt% Fe, the E_{OCP} value shifts significantly in the anodic direction by adding molybdenum (Figure 5). With an iron content of 1.5 wt% Fe, however, no change in the corrosion potential is observed. An influence on the protective effect and the electrochemical stability of the coatings caused by the addition of molybdenum cannot be determined on the basis of the R_L values (Figure 6). The ternary coatings thus exhibit the same protective effect and stability in the initial state as the binary coatings. The results of the EIS show that the addition of molybdenum does not result in any significant change in the electrochemical properties of the coatings in the initial state (Figure 7). The ternary coatings with an additional molybdenum content thus only differ from the binary coatings regarding the E_{OCP} value at low molybdenum contents. In contrast, the protective effect, electrochemical stability, and structure of the coating system are not significantly influenced.

4.2. Influence of Additional Passivation Layer

The iron-containing binary and ternary coatings were provided with an additional passivation layer by applying a passivating agent. This additional layer can be reliably identified by means of EIS, as it has a significant influence on the impedance spectrum and the phase shift (Figure 7). The fit by means of an equivalent circuit model (Table 2) shows that an additional layer can be measured in the structure of the coating.

The additional passivation initially has a noticeable influence on the E_{OCP} values (Figure 4 and 5). The potentials, with the exception of the coating ZnFeMo(0.6%Fe), are 50–80 mV more anodic compared to the coatings without passivation. There is a recognizable trend that the E_{OCP} value of the passivated coatings becomes more anodic with increasing alloy content of iron and molybdenum. However, no statements can be made about the protective effect of the coatings from the E_{OCP} values. The advantages of an additional passivation of the coatings are shown in Figure 6. The passivation has a significant influence on the protective effect and the electrochemical stability of the coatings, represented by the R_L value. The passivated coatings have an R_L value that is tenfold higher than the respective untreated coatings. They are more electrochemically stable. Passivation can thus initially provide very good protection, which is reflected in high R_L values. These values are in a range that can also be measured by means of natural weathering over longer periods of time on a pure zinc surface, whereby very protective corrosion products are formed.^[2,23] An influence of additional passivation on surface morphology and coating thickness was not visible (Figure 2 and 3).

4.3. Influence of Artificial Aging on Layer Formation and Degradation

Artificial aging was employed to investigate how the different coatings change within a certain weathering period due to the influence of a wet/dry cycle. The changes in surface morphology and corrosion defects of the coatings can be evaluated by comparing Figure 2 and 3 (initial state) to Figure 8 and 9 (after 21 days of artificial aging). Coatings without post-treatment are covered with corrosion products and show signs of corrosion as well as defects that reach down to the substrate after artificial aging. Defects themselves are covered with corrosion products. Coatings with an additional passivation show no signs of a corrosion product layer. Nevertheless, defects that reach down to the steel substrate are also visible. Looking at the E_{OCP} values in Figure 10, the coatings are subject to changes due to weathering. With increasing weathering time, there is a tendency for the potentials to shift in anodic direction. For the non-passivated coatings, it is an indication of layer formation from corrosion products on the surface. For the passivated coating, it is an indication of possible degradation of the passivation layer. The results of the EIS in Figure 12 and their evaluation in Table 3 confirm these assumptions. The layers of the coatings ZnFeMo(0.6%Fe) without post-treatment and ZnNi(8%Ni) are subject to a significant change in the structure during the 21 days of artificial aging, as the equivalent circuit models in Figure 1 show. With increasing aging time, an additional layer of

corrosion products is added, which has a positive effect on the protective effect and electrochemical stability according to the R_L values in Figure 11. The passivated variant of ZnFeMo(0.6%Fe), on the other hand, does not change with regard to its basic structure and even after 21 days the same layer system as in the initial state can still be approximated by means of equivalent circuit models. A more detailed insight into the development of the protective effect is provided by the R_L values as a function of aging time in Figure 11. The protective effect increases significantly for the ZnFeMo(0.6%Fe) coating without post-treatment and the ZnNi(8%Ni) coating up to a period of 14 days, respectively. R_L values are measured that are almost tenfold above the values in the initial state. Afterward, the protective effect decreases slightly, as corrosion products can continue to transform due to the influence of the wet/dry cycle. The passivated coating provides very high R_L values at the beginning of artificial aging and thus a very high electrochemical stability of the passivation layer. However, the passivation layer appears to degrade with increasing aging time and to decrease in its protective effect. It is accompanied by the formation of defects that reach down to the steel substrate. Nevertheless, the protective effect remains higher than without additional passivation within the 21 days of weathering considered. The non-passivated surfaces reach the level of the passivated surfaces for only a short time. One reason for this could be that the rainfall that is necessary for the formation of very well-protective corrosion products does not occur in the artificial aging cycle.^[23,25]

The following ranking of the R_L values of the coatings after 21 days of weathering is given:

(high R_L)	ZnFeMo(0.6%Fe), passivated	
	>ZnNi(8%Ni)	
	>ZnFeMo(0.6%Fe), without post-treatment	(low R_L)

Nevertheless, the ZnNi(8%Ni) coating and the ZnFeMo(0.6%Fe) coating without post-treatment are of a similar order of magnitude and thus also exhibit a similar protective effect. However, a statement on the long-term behavior cannot be derived due to the short weathering times.

5. Conclusion

The objective of the electrochemical investigations was to characterize the corrosion protection and electrochemical stability of nickel-free binary and ternary zinc coatings in comparison to a nickel-containing type. The electrochemical investigations were carried out by means of gel electrolytes to reduce the influence of the test medium on the zinc-containing coatings, which would lead to a change in the surface layers during the investigation (minimally invasive approach). The study revealed the following findings: 1) The protective effect, electrochemical stability, and structure of the coatings are not affected by different iron contents of 0.6 and 1.5 wt% Fe. 2) The addition of molybdenum with contents of 0.3–0.5 wt% Mo to binary ZnFe coatings does not lead to an improvement of the protective effect and the electrochemical stability. 3) The protective effect of binary and ternary ZnFe-containing coatings is similar to that of a ZnNi coating in the unweathered state, respectively. 4) Passivation of the

ZnFe-containing coatings by means of a passivating agent leads to an improvement of the protective effect and the electrochemical stability. The passivated coatings have a Corrosion product layer resistance R_L that is tenfold higher. 5) Artificial aging leads to the formation of corrosion products on the surface of non-passivated coatings, which is accompanied by an increase in

the protective effect and electrochemical stability. 6) Artificial aging leads to a slight degradation of the passivation layer of passivated coatings accompanied by a decreasing Corrosion product layer resistance R_L . 7) ZnFeMo-containing coatings show a similar protective effect as a ZnNi coating, even after 21 days of artificial aging.

Table A1. Results of the EIS fit with (A) equivalent circuit model including a coating layer.

Coating	$\frac{R_{el}}{[\Omega]}$	$\frac{R_{layer\ 1}}{[\Omega]}$	$\frac{R_p}{[\Omega]}$	$\frac{Y_{o_layer\ 1}}{[S * s^2]}$	$a_{layer\ 1}$	$\frac{Y_{o_CPE}}{[S * s^2]}$	a_{CPE}
ZnFe(0.6%Fe) coating without post-treatment initial state	49.9	5.6 k	1.1 k	72.4 μ	0.8	1,300 μ	1.0
ZnFe(1.5%Fe) coating without post-treatment initial state	35.9	5.4 k	0.8 k	89.3 μ	0.8	1,400 μ	1.0
ZnFeMo(0.6%Fe) coating without post-treatment initial state	58.7	6.6 k	0.2 k	69.0 μ	0.9	2,900 μ	1.0
ZnFeMo(1.5%Fe) coating without post-treatment initial state	66.1	4.9 k	1.2 k	80.0 μ	0.8	900 μ	1.0
ZnNi(8%Ni) coating without post-treatment initial state	69.4	0.5 k	6.7 k	21.6 μ	0.9	61.4 μ	0.6

Table A2. Results of the EIS fit with (B) equivalent circuit model including a coating layer and a diffusion component.

Coating	$\frac{R_{el}}{[\Omega]}$	$\frac{R_{layer\ 1}}{[\Omega]}$	$\frac{R_p}{[\Omega]}$	$\frac{Y_{o_layer\ 1}}{[S * s^2]}$	$a_{layer\ 1}$	$\frac{Y_{o_CPE}}{[S * s^2]}$	a_{CPE}	$\frac{W_D}{[S * s^{1/2}]}$
ZnFeMo(0.6%Fe) coating without post-treatment aged 1 day	42.7	1.5 k	2.7 k	56.7 μ	0.8	162.2 μ	0.8	9,700 μ
ZnNi(8%Ni) coating without post-treatment aged 1 day	48.3	1.2 k	7.8 k	9.7 μ	0.9	390.3 μ	1.0	79.1 μ
ZnNi(8%Ni) coating without post-treatment aged 7 days	44.2	0.9 k	68.3 k	2.9 μ	0.9	209.3 μ	0.3	59.2 μ

Table A3. Results of the EIS fit with (C) equivalent circuit model including several layers.

Coating	$\frac{R_{el}}{[\Omega]}$	$\frac{R_{layer\ 1}}{[\Omega]}$	$\frac{R_{layer\ 2}}{[\Omega]}$	$\frac{R_p}{[\Omega]}$	$\frac{Y_{o_layer\ 1}}{[S * s^2]}$	$a_{layer\ 1}$	$\frac{Y_{o_layer\ 2}}{[S * s^2]}$	$a_{layer\ 2}$	$\frac{Y_{o_CPE}}{[S * s^2]}$	a_{CPE}
ZnFe(0.6%Fe) coating + passivation initial state	50.0	4.0 k	1,500 k	0.2 k	2.1 μ	0.9	24.1 μ	0.6	7.7 μ	1.0
ZnFe(1.5%Fe) coating + passivation initial state	67.2	0.9 k	45.5 k	191.6 k	1.5 μ	1.0	32.5 μ	0.5	12.6 μ	0.8
ZnFeMo(0.6%Fe) coating + passivation initial state	48.2	0.8 k	73.7 k	97.0 k	1.8 μ	1.0	43.4 μ	0.4	26.8 μ	0.8
ZnFeMo(1.5%Fe) coating + passivation initial state	49.1	2.5 k	1,300 k	4.4 k	2.1 μ	0.9	19.9 μ	0.6	34.2 μ	1.0
ZnFeMo(0.6%Fe) coating without post-treatment aged 7 days	14.1	0.7 k	18.7 k	17.4 k	1.5 μ	1.0	43.5 μ	0.5	2,300 μ	1.0
ZnFeMo(0.6%Fe) coating without post-treatment aged 14 days	75.8	21.0 k	69.0 k	4.9 k	8.0 μ	0.8	66.1 μ	0.7	6.4 μ	0.8
ZnFeMo(0.6%Fe) coating without post-treatment aged 21 days	34.5	1.9 k	5.9 k	65.8 k	6.3 μ	0.8	24.0 μ	0.6	79.6 μ	0.7
ZnFeMo(0.6%Fe) coating + passivation aged 1 day	43.6	1.9 k	531.3 k	0.1 k	0.9 μ	1.0	10.2 μ	0.6	9,000 μ	0.6
ZnFeMo(0.6%Fe) coating + passivation aged 7 days	37.6	1.3 k	28.6 k	188.7 k	1.1 μ	1.0	18.2 μ	0.6	21.3 μ	0.9
ZnFeMo(0.6%Fe) coating + passivation aged 14 days	56.0	1.6 k	3,700 k	1.8 k	1.1 μ	1.0	13.3 μ	0.6	9,900 μ	0.3
ZnFeMo(0.6%Fe) coating + passivation aged 21 days	37.4	0.5 k	18.4 k	312.8 k	1.0 μ	1.0	34.6 μ	0.5	28.5 μ	0.8
ZnNi(8%Ni) coating without post-treatment aged 14 days	50.8	0.9 k	99.0 k	8.2 k	1.3 μ	1.0	25.3 μ	0.5	39.1 μ	0.8

Table A4. Results of the EIS fit with (D) equivalent circuit model including several layers and a diffusion component.

Coating	$\frac{R_{el}}{[\Omega]}$	$\frac{R_{layer\ 1}}{[\Omega]}$	$\frac{R_{layer\ 2}}{[\Omega]}$	$\frac{R_p}{[\Omega]}$	$\frac{Y_{o_layer\ 1}}{[S * s^2]}$	$a_{layer\ 1}$	$\frac{Y_{o_layer\ 2}}{[S * s^2]}$	$a_{layer\ 2}$	$\frac{Y_{o_CPE}}{[S * s^2]}$	a_{CPE}	$\frac{W_D}{[S * s^{1/2}]}$
ZnNi(8%Ni) coating without post-treatment aged 21 days	40,4	1.5 k	1,200 k	0.2 k	2.4 μ	1.0	25.5 μ	0.5	3.9 μ	1.0	6,100 μ

Annex

EIS fitting was carried out with Gamry Echem Analyst Software by using the Simplex method. The results of fitting are summarized in the following Table A1, A2, A3, and A4 sorted by equivalent circuit model.

R_L determined by linear polarization does not equal the pure R_p as determined by fitting of EIS results. As a sum of all resistances, R_L contains the electrolyte resistance, the different layer resistances, charge transfer resistance, and the resistance of the corrosion product film according to Langklotz et al.^[2]

Thus, R_L is in accordance with the sum of all resistances determined by EIS fitting since an analogous behavior in dependence of coating type and artificial aging time can be seen for all investigated samples. Valet et al. have shown that R_L values correspond well to EIS results and to the overall protective ability of zinc coatings and their respective corrosion products.^[23]

Acknowledgements

The authors gratefully acknowledge funding by the German Federal Ministry of Education and Research (BMBF) and the project carrier VDI Technologiezentrum GmbH within the joint project 13XP5031E. The authors also gratefully acknowledge funding by the Federal Ministry for Economic Affairs and Energy and the project carrier Projektträger Jülich within the WIPANO project GELELEK, FKZ 03TNH014A.

Open access funding enabled and organized by Projekt DEAL.

Conflict of Interest

The authors declare no conflict of interest.

Data Availability Statement

The data that support the findings of this study are available from the corresponding author upon reasonable request.

Keywords

binary zinc alloys, corrosion testing, gel electrolytes, ternary zinc alloys

Received: September 29, 2021

Revised: January 21, 2022

Published online:

- [1] S. C. Chung, S. L. Sung, C. C. Hsien, H. C. Shih, *J. Appl. Electrochem.* **2000**, *30*, 607.
- [2] U. Langklotz, M. Babutzka, M. Schneider, A. Burkert, *Mater. Corros.* **2019**, *70*, 1314.
- [3] D. Thierry, N. LeBozec, A. Le Gac, D. Persson, *Mater. Corros.* **2019**, *70*, 2220.
- [4] X. Zhang, C. Leygraf, I. Odnevall Wallinder, *Corros. Sci.* **2013**, *73*, 62.
- [5] H. Dafydd, D. A. Worsley, H. N. McMurray, *Corros. Sci.* **2005**, *47*, 3006.
- [6] D. Thierry, D. Persson, G. Luckeneder, K.-H. Stellnberger, *Corros. Sci.* **2019**, *148*, 338.
- [7] J. Stoullil, T. Prosek, A. Nazarov, J. Oswald, P. Kriz, D. Thierry, *Mater. Corros.* **2015**, *66*, 777.
- [8] R. Morgenstern, M. Müller, D. Höhlich, T. Mehner, T. Lampke, *IOP Conf. Ser.: Mat. Sci. Eng.* **2021**, *1147*, 012004.
- [9] J. R. Vilche, K. Jüttner, W. J. Lorenz, W. Kautek, W. Paatsch, M. H. Dean, U. Stimming, *J. Electrochem. Soc.* **1989**, *136*, 3773.
- [10] W. Kautek, M. Sahre, W. Paatsch, *Electrochim. Acta* **1994**, *39*, 1151.
- [11] H. Kazimierczak, J. Morgiel, Z. Swiatek, J. M. Vega, E. García-Lecina, *Corros. Sci.* **2018**, *135*, 107.
- [12] J. Winiarski, W. Tylus, A. Lutz, I. De Graeve, B. Szczygiel, *Corros. Sci.* **2018**, *138*, 130.
- [13] W. Paatsch, R. Morgenstern, H. Sahrhage, G. Mollath, T. Lampke, *Trans. IMF* **2021**, *99*, 227.
- [14] BSI British Standards, *Zinc Coatings—Guidelines and Recommendations for the Protection Against Corrosion of Iron and Steel in Structures—Part 1: General Principles of Design and Corrosion Resistance*, ISO 14713-1:2017, German version EN ISO 14713-1:2017, BSI British Standards, London **2017**.
- [15] Standards South Africa, *Corrosion Tests in Artificial Atmospheres—Salt Spray Tests*, ISO 9227:2017, German version EN ISO 9227:2017, Standards South Africa, Pretoria.
- [16] K. Bartoň, D. Čermáková, *Werkst. Korros.* **1964**, *15*, 374.
- [17] N. LeBozec, N. Blandin, D. Thierry, *Mater. Corros.* **2008**, *59*, 889.
- [18] E. Cano, A. Crespo, D. Lafuente, B. Ramirez Barat, *Electrochem. Commun.* **2014**, *41*, 16.
- [19] C. J. Newton, J. M. Sykes, *Corros. Sci.* **1988**, *28*, 1051.
- [20] G. Monrrabal, B. Ramírez-Barat, A. Bautista, F. Velasco, E. Cano, *Metals* **2018**, *8*, 500.
- [21] G. Monrrabal, S. Guzmán, I. E. Hamilton, A. Bautista, F. Velasco, *Electrochim. Acta* **2016**, *220*, 20.
- [22] M. Babutzka, A. Heyn, *IOP Conf. Ser.: Mat. Sci. Eng.* **2017**, *181*, 012021.
- [23] S. Valet, A. Burkert, G. Ebell, M. Babutzka, *Electrochim. Acta* **2021**, *385*, 138191.
- [24] G. Monrrabal, A. Bautista, F. Velasco, *Corrosion* **2019**, *75*, 1502.
- [25] M. Babutzka, Dissertation, RWTH Aachen University, August, **2021**.